Sensors and Materials, Vol. 38, No. 2 (2026) 609–619
MYU Tokyo

S & M 4329

Radiation-induced Optical Responses of Ag Centers in $NaCaPO_4$ Ceramics

Yamato Saotome,[1] Daiki Shiratori,[1*] Yutaka Fukuchi,[1] and Hiromi Kimura[2]

[1]Tokyo University of Science (TUS), 6-3-1 Niijuku, Katsushika, Tokyo 125-8585, Japan
[2]National Metrology Institute of Japan, National Institute of Advanced Industrial Science and Technology (AIST), 1-1-1 Umezono, Tsukuba, Ibaraki 305-8568, Japan

(Received October 30, 2025; accepted December 17, 2025)

Keywords: ceramics, photoluminescence, dosimeter, radio-photoluminescence, radiochromism

In this study, we investigated the radiation-induced optical responses of $NaCaPO_4$ ceramics doped with Ag (0.1, 0.3, 1.0, 2.0, and 3.0%). After irradiating the samples with X-rays, the photoluminescence (PL) recorded under UV excitation increased slightly at low doses (≤~100 mGy), which is indicative of the radio-photoluminescence (RPL) phenomenon. At higher doses (≥~1 Gy), the PL intensity decreased. Prompted by the high-dose PL quenching, we measured the reflection spectra, which revealed that absorption bands were induced by X-ray irradiation and that their intensities increased with absorbed dose. In particular, the band centered at ~400 nm, attributable to the surface plasmon resonance of Ag nanoparticles, grew monotonically with absorbed dose. The 0.3% Ag-doped sample provided an exceptionally broad dynamic range from ~1 mGy to 100 Gy. These results indicate that the Ag-doped $NaCaPO_4$ ceramic is more appropriately regarded as a radiochromic material than as an RPL phosphor and is well suited to applications requiring wide-range dose monitoring.

1. Introduction

The accurate measurement of ionizing radiation dose is essential in various fields, including medical therapy,[1,2] industrial applications,[3,4] and personnel radiation protection.[5–9] For these purposes, passive-type detectors (dosimeters) are widely used, with storage phosphors and radiochromic materials being the most common classes. For routine operational dose monitoring, storage-phosphor dosimetry is conducted using thermally stimulated luminescence (TSL) materials, such as LiF:Mg,Ti (TLD-100),[10] $CaSO_4$:Dy,[11] or LiF:Mg,Cu,P,[12] and optically stimulated luminescence (OSL) materials, such as Al_2O_3:C[13] or BeO.[14] For imaging applications, storage-phosphor screens (imaging plates) based on OSL materials such as BaFBr:Eu^{2+}[15] or CsBr:Eu^{2+}[16] provide high-dynamic-range X-ray detection. Within the same storage-phosphor family, radio-photoluminescence (RPL) is employed primarily for personal and environmental dose monitoring, typically using Ag-activated phosphate glass in which irradiation creates stable luminescent centers that can be read optically and, in principle,

*Corresponding author: e-mail: shiratori@rs.tus.ac.jp
https://doi.org/10.18494/SAM6080

ISSN 0914-4935
https://myukk.org/

reread.[17,18] In clinical radiotherapy, radiochromic films (e.g., Gafchromic EBT series) are routinely used to map two-dimensional dose distributions with sub-millimeter resolution during patient-specific quality assurance and beam commissioning.[19]

These dosimetry methods rely on different physical phenomena induced by ionizing radiation. In storage phosphors, ionizing radiation generates charge carriers, and these carriers are stored as trapped carriers at trapping centers (for example, intrinsic or impurity-related sites). When an external stimulus releases the trapped carriers, they recombine at luminescence centers and emit light. Emission produced by heating is called TSL,[20–24] and emission produced by optical excitation is called OSL.[20,25–27] RPL is the phenomenon in which ionizing radiation generates new luminescent centers that retain dose information.[28–33] In Ag-activated glasses, radiation-generated carriers drive redox reactions among Ag species (for example, conversion of Ag^+ to Ag^0, Ag^{2+}, and the formation of small Ag clusters), and these Ag-related species act as luminescent centers that can be read out optically with minimal depletion of the stored information. Distinct from these luminescence-based methods, radiochromism is a phenomenon where a material changes its optical absorption properties upon irradiation.[34,35] This change arises from the formation of stable absorption centers (color centers), including defects and aggregated species such as atomic clusters or nanoparticles that absorb in the visible and adjacent near-UV or near-IR range. A representative mechanism involves radicals generated by irradiation converting colorless precursors into stable chromophores via oxidation or bond rearrangement, thereby producing a dose-dependent increase in absorbance. In addition, radiochromic systems that utilize coloration arising from the irradiation-induced clustering of Ag exist. In these materials, in contrast to the RPL response, the Ag-related absorption increases with dose and serves as the measurable signal.

Against this backdrop, we adopt Ag as a radiation-responsive probe and select thermally and chemically robust $NaCaPO_4$ as the host.[36,37] Eu-doped compositions show strong photoluminescence (PL) and have been explored as white phosphors.[38,39] Moreover, in related $ABPO_4$ (A = alkali metal, B = alkaline-earth metal) hosts, RPL arising from irradiation-induced changes in Eu valence has been reported, indicating that cation redox can be driven by ionizing radiation in these materials.[40] These observations motivate the hypothesis that, in $NaCaPO_4$, Ag may likewise undergo irradiation-induced valence change and/or aggregation (clustering), potentially yielding both RPL emission and/or radiochromic absorption within the same material system. Therefore, in this study, we evaluated the dosimetric characteristics of Ag-doped $NaCaPO_4$ ceramics to reveal whether they qualify as a storage-phosphor candidate.

2. Materials and Methods

2.1 Sample preparation

The Ag-doped $NaCaPO_4$ ceramic samples were synthesized by a conventional solid-state reaction method. The starting materials were Na_2CO_3 (99.8%, Fujifilm Wako Pure Chemical Corporation), $CaCO_3$ (99.5%, Fujifilm Wako Pure Chemical Corporation), $NH_4H_2PO_4$ (99.0%, Fujifilm Wako Pure Chemical Corporation), and Ag_2O (Wako Special Grade, Fujifilm Wako

Pure Chemical Corporation). Stoichiometric amounts of these powders were weighed to prepare compositions of $Na(Ag_xCa_{1-x})PO_4$ with x = 0.001, 0.003, 0.01, 0.02, and 0.03, aiming for a total batch weight of 3.000 g. The weighed powders were thoroughly mixed using an agate mortar and a pestle. The mixed powder was then calcined in an electric furnace at 900 ºC for 3 h in an air atmosphere. The heating rate was approximately 15 ºC/min, and the sample was cooled naturally in the furnace. After calcining, the resulting product was ground again and pressed into pellets (1 cm diameter) by applying a uniaxial pressure of 20 MPa for 20 min using a press machine (Mini-Lab-Press, Labnect Co., Ltd.) without the use of binders. Finally, the pellets were sintered at 900 ºC for 1 h in an air atmosphere with a heating rate of 15 ºC/min, followed by furnace cooling.

2.2 Methods

The crystal structure of the synthesized samples was determined by X-ray diffraction (XRD) analysis using a diffractometer (MiniFlex600, Rigaku). PL excitation and emission spectra were measured using a spectrofluorometer (FP-8550, JASCO Corporation). Emission spectra (λ_{ex} = 230 nm; 260–500 nm) and excitation spectra (λ_{em} = 300 nm; 200–280 nm) were recorded with excitation/emission bandwidths of 2.5 nm and a 1 nm step size. Reflection spectra were measured with ~45° illumination and normal (0°) collection using a fiber-coupled reflection probe (RPH-1, Ocean Optics), as shown in Fig. 1. Incident light from a xenon lamp (E7536, Hamamatsu) was delivered to the sample via an optical fiber and adaptor (A11096, Hamamatsu), and the specularly reflected light was collected through a fiber and analyzed with a spectrometer (QEPro, Ocean Optics). To ensure the stability of the excitation source, the xenon lamp was warmed up for approximately 1 h before the measurements. Polytetrafluoroethylene (PTFE; WS-1, Ocean Optic) was used as the reflectance standard. Each sample spectrum was normalized to the PTFE spectrum, and the relative reflectance loss $C(\lambda)$ at wavelength λ was calculated using the following equation.

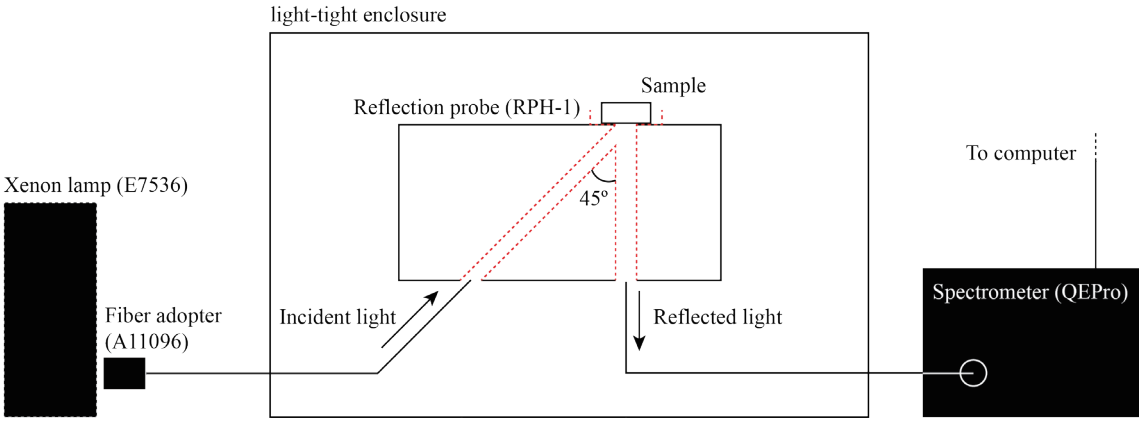

Fig. 1. (Color online) Schematic of the reflection spectra measurement setup.

$$C(\lambda) = 1 - \frac{R_{sample}(\lambda)}{R_{PTFE}(\lambda)} \tag{1}$$

Here, $R_{sample}(\lambda)$ and $R_{PTFE}(\lambda)$ denote the measured reflectance of the sample and the PTFE reference, respectively. To investigate the radiation-induced effects, the samples were irradiated with X-rays using an X-ray generator (G511VL-D, Canon Anelva) operated at a tube voltage of 40 kV. The irradiation dose, ranging from 0.01 mGy to 100 Gy, was controlled by adjusting the tube current (10–100 μA), irradiation time, and distance. Dose calibration was performed using an ionization chamber (TN31013, PTW) and an electrometer (EMF521A, EMF Japan). After X-ray irradiation, the changes in the PL and reflection spectra were measured under the same conditions as mentioned above.

3. Results and Discussion

Figure 2 shows the powder XRD patterns of the Ag-doped $NaCaPO_4$ ceramic samples with the reference pattern of $NaCaPO_4$ from the Inorganic Crystal Structure Database (ICSD). In every sample, the $NaCaPO_4$ phase is dominant, confirming that the target crystal structure has essentially been obtained. On the other hand, faint extra reflections are observed near 2θ = ~30º, which can be reasonably assigned to $Na_2CaP_2O_7$ (ICSD No. 89468)[41] and Ag_3PO_4 (ICSD No. 14000).[42] These traces suggest that the solid solubility of Ag on the Ca site in the solid state reaction route is limited.

Figure 3(a) shows the normalized PL excitation and emission spectra of the Ag-doped $NaCaPO_4$ ceramic samples. Focusing first on the ultraviolet emission bands, all samples exhibit characteristic broad emission bands centered at ~280 and ~300 nm under 230 nm excitation.

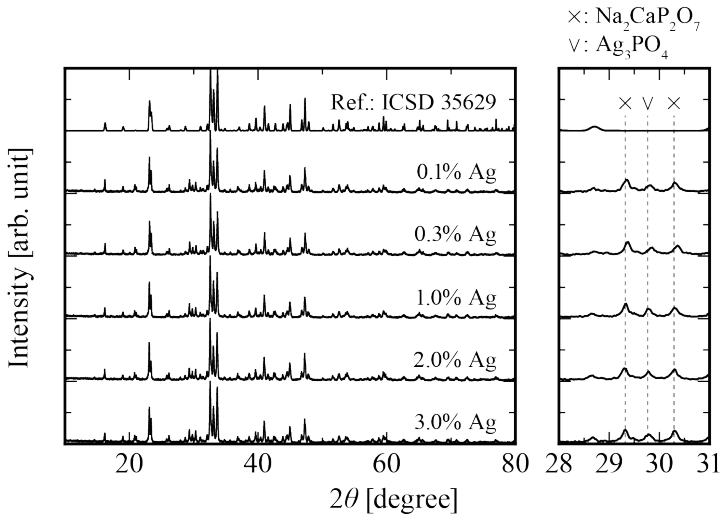

Fig. 2. (Color online) Powder XRD patterns of the Ag-doped $NaCaPO_4$ ceramic samples together with the reference pattern of $NaCaPO_4$ (ICSD No. 35629). The right panel shows an enlarged view at 2θ = 28–31°.

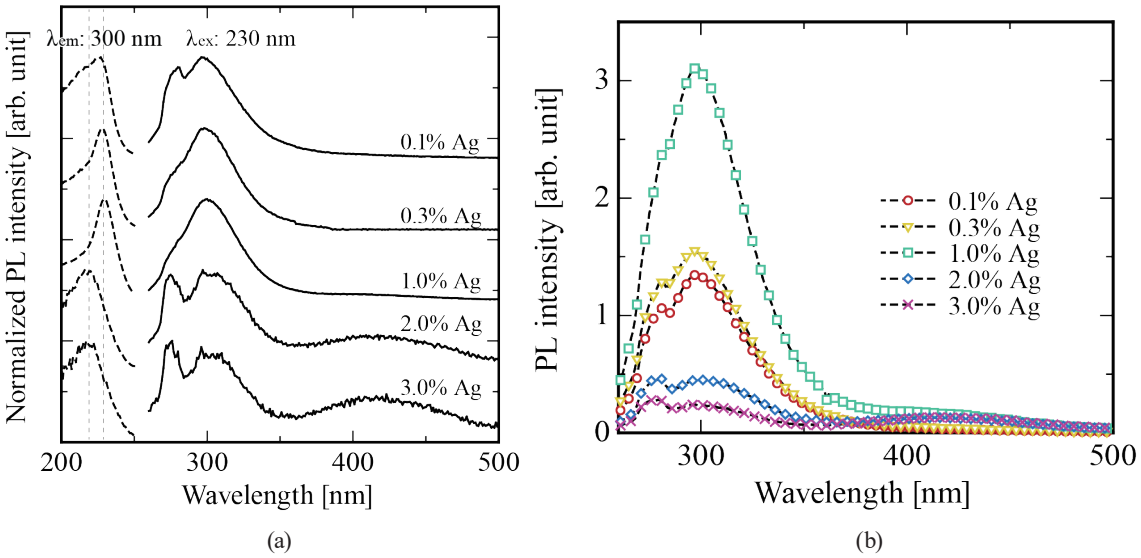

Fig. 3. (Color online) (a) Normalized PL excitation and emission spectra and (b) PL emission spectra of Ag-doped $NaCaPO_4$ ceramic samples. Excitation wavelength for emission spectra and monitored wavelength for excitation spectra are 230 and 300 nm, respectively.

Emission near 300 nm is generally associated with Ag^+ ions.[17,43–45] The apparent double-peak structure of the UV emission can be reasonably explained by two contributions: (i) emissions from Ag^+ centers occupying at least two distinct local environments within $NaCaPO_4$, and (ii) the presence of an absorption band near ~280 nm that overlaps the emission envelope and yields an apparent splitting. These two effects are not mutually exclusive. The contribution of case (ii) is further addressed in the reflection spectra section. The relative intensities of these bands depend on the Ag concentration: in the 0.3 and 1.0% Ag-doped samples, the 300 nm band is predominant, whereas in the 0.1, 2.0, and 3.0% Ag-doped samples, the 280 nm band dominates. In concert with this trend, the excitation spectra show that the ~230 nm excitation band is predominant for the 0.3 and 1.0% Ag-doped samples. In contrast, the ~220 nm excitation band is predominant for the other compositions. Accordingly, the 300 nm emission is preferentially excited via the ~230 nm band, whereas the 280 nm emission is preferentially excited via the ~220 nm band. In addition to these ultraviolet bands, a broad emission band is observed around 430 nm. According to previous studies, this emission can be attributed to isolated Ag^0 and/or Ag_2^+.[33,46–49] Figure 3(b) shows the PL emission intensities of all Ag-doped $NaCaPO_4$ ceramic samples under 230 nm excitation. The highest PL intensity was observed for the 1.0% Ag-doped sample, whereas samples with higher concentrations exhibited significantly weaker emission. The decrease in emission intensity is plausibly attributable to concentration quenching and/or to the clustering-induced depletion of Ag^+ centers accompanied by enhanced self-absorption. These observations indicate that changes in Ag concentration primarily affect the 300 nm emission component, and its optimum Ag content for maximizing the PL intensity is around 1.0%.

Figure 4 presents the evolution of the PL spectra of all Ag-doped $NaCaPO_4$ ceramic samples as the X-ray dose was swept from 0.1 mGy to 10 Gy. Across all samples, the main emission band shows a slight increase in intensity in the low-dose range (≤~100 mGy), whereas at higher doses

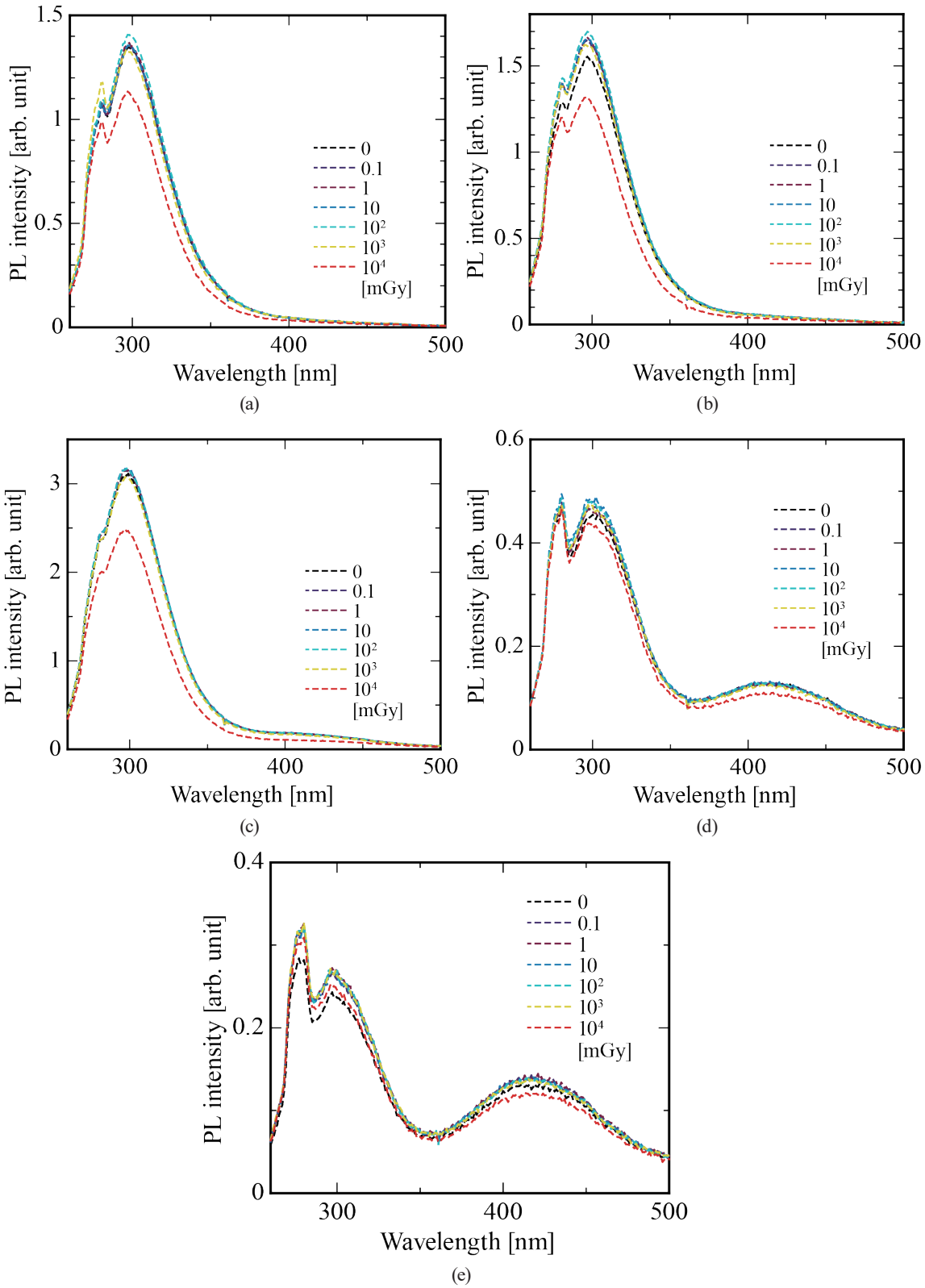

Fig. 4. (Color online) PL spectra of $NaCaPO_4$ ceramic samples with Ag concentrations of (a) 0.1%, (b) 0.3%, (c) 1.0%, (d) 2.0%, and (e) 3.0%, recorded after X-ray irradiation over the range of 0.1 mGy–10 Gy.

(≥~1 Gy), the trend reverses and the intensities decrease. The increase of ~300 nm emission suggests that holes generated by X-ray irradiation are captured by Ag^0, oxidizing it to Ag^+. Accordingly, the observed increase in PL intensity suggests the occurrence of RPL in these compositions. By contrast, the decrease in luminescence at higher doses can be attributed to concentration quenching as the population of RPL centers (Ag^+) grows and/or to additional absorption associated with surface plasmon resonance (SPR) arising from the progressive aggregation of Ag^0 into clusters.

Figures 5(a)–5(e) show the changes in the reflection spectra of Ag-doped $NaCaPO_4$ ceramic samples as the X-ray dose is varied. In the following, we denote the relative reflectance loss at wavelength λ and irradiation dose D as $C(\lambda, D)$, with $C(\lambda, D_0)$ corresponding to the unirradiated state (D_0 = 0 Gy). In all the samples before X-ray irradiation, absorption bands are observed at ~250 and 400 nm. The ~250 nm feature has been reported for Ag clusters such as $[Ag_2]^{2+}$,[50–52] and may contribute to the apparent splitting of the ultraviolet PL band noted above. In contrast, the ~400 nm band is characteristic of the SPR of Ag nanoparticles.[50,53,54] The intensities of both bands tend to increase with Ag content; in highly doped samples, this likely reflects the partial aggregation of Ag during the synthesis process, yielding a larger nanoparticle population. Upon X-ray irradiation, both absorption intensities continue to increase. The ~400 nm band shows the largest change, indicating the radiation-induced reduction of Ag^+ to Ag^0 and the subsequent formation of Ag nanoparticles. In highly Ag-doped samples, the incremental change is smaller, likely because nanoparticles are already abundant from the synthesis process. These results indicate that the present samples exhibit a clear radiochromic response. Figure 5(f) shows the dose dependence of the radiation-induced reflectance change $\Delta C(D)$ (radiochromic response). Here, $\Delta C(D)$ denotes the reflectance change integrated over the wavelength range of 300–500 nm, obtained from the wavelength-dependent radiation-induced reflectance change $\Delta C(\lambda, D)$, which is defined as

$$\Delta C(\lambda, D) = C(\lambda, D) - C(\lambda, D_0)\,. \tag{2}$$

In all the samples, $\Delta C(D)$ increases with irradiation dose above approximately 1 Gy. Notably, the 0.3% Ag-doped sample exhibits the most favorable behavior for the dosimeter, showing a monotonic increase in absorption over a broad range from ~1 mGy to 100 Gy without obvious saturation. For context, commercial radiochromic dosimeters report lower detectable doses on the order of ~0.2 Gy for Gafchromic EBT3 (radiotherapy range),[55] ~1–200 mGy for Gafchromic XR-QA2 (diagnostic range),[56] and ~0.1 Gy for representative PRESAGE formulations.[57] Thus, the 0.3% Ag-doped $NaCaPO_4$ ceramic appears to be a promising radiochromic material that exhibits mGy-level sensitivity while maintaining a wide dynamic range under X-ray irradiation.

Figure 6 shows the dose dependences of the integrated PL intensity change ΔI_{PL} and the radiochromic response $\Delta C(D)$ for the 0.3% Ag-doped sample. Here, ΔI_{PL} is defined as the difference between the integrated PL intensity over the wavelength range (260–500 nm) at a given dose and that of the unirradiated sample (0 Gy). The ΔI_{PL} values show a slight increase with irradiation dose in the low-dose region (<100 mGy), mainly owing to the contribution of the RPL phenomenon. When the dose exceeds about 1 Gy, however, the radiation-induced formation

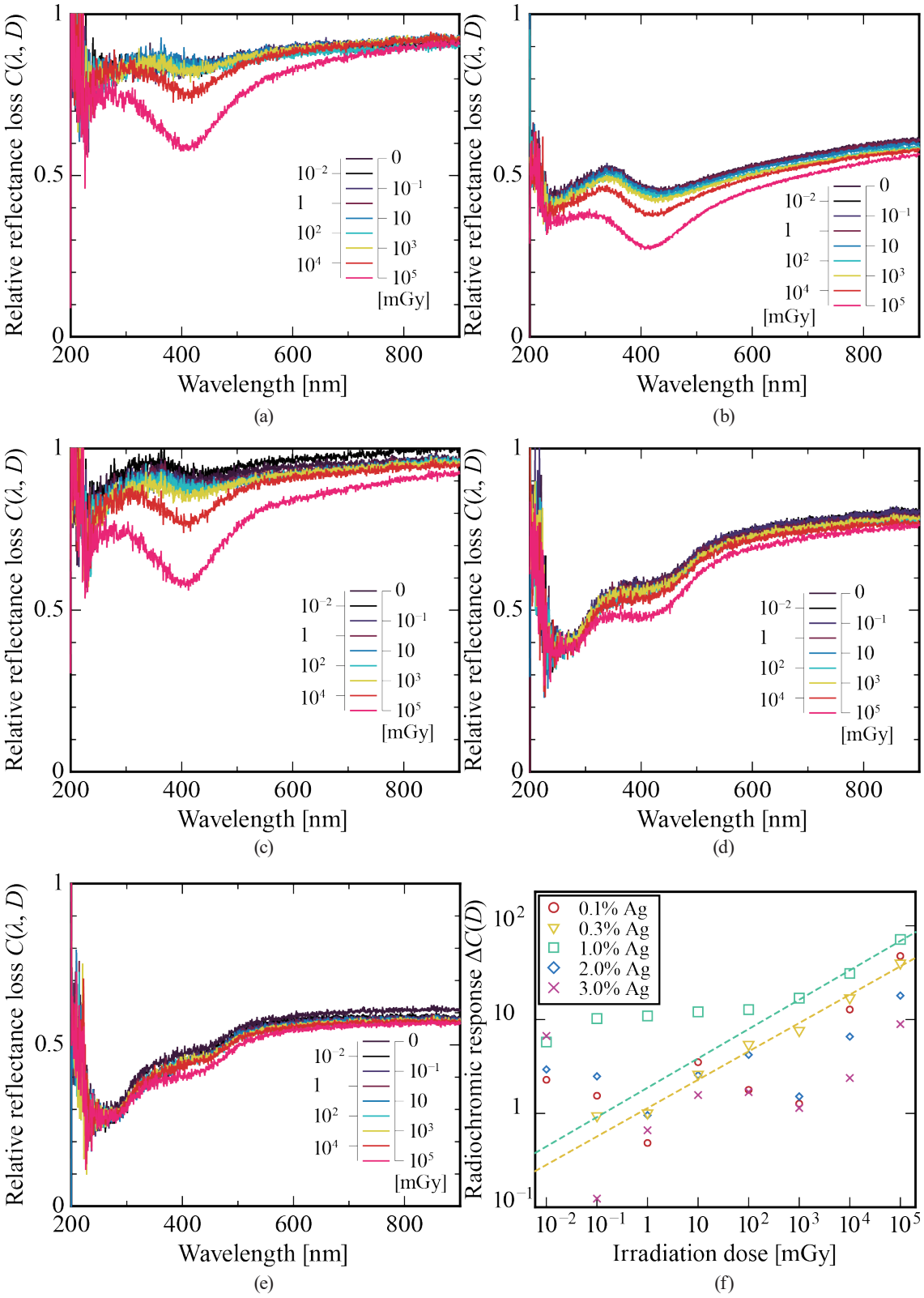

Fig. 5. (Color online) Reflection spectra of $NaCaPO_4$ ceramics with Ag concentrations of (a) 0.1%, (b) 0.3%, (c) 1.0%, (d) 2.0%, and (e) 3.0% recorded after X-ray irradiation over the range of 0.01 mGy–100 Gy. (f) Integrated radiation-induced reflectance change $\Delta C(D)$ plotted as a function of irradiation X-ray dose.

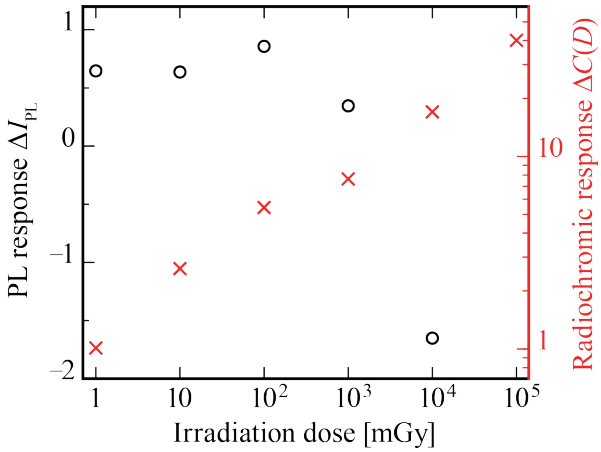

Fig. 6. (Color online) Dose-response curves for PL response ΔI_{PL} (circles, left axis) and radiochromic response $\Delta C(D)$ (crosses, right axis) for the 0.3% Ag-doped sample.

of Ag clusters and nanoparticles becomes dominant, and Ag^+ centers are progressively incorporated into these non-emissive species. Consequently, the number of PL-active Ag^+ centers decreases and ΔI_{PL} is reduced, resulting in a non-monotonic dose dependence. In contrast, $\Delta C(D)$ (crosses), which arises from the surface plasmon resonance of Ag nanoparticles, increases monotonically from 1 mGy to 100 Gy, consistent with the progressive growth and accumulation of Ag nanoparticles already in the low-dose region. Thus, although both signals arise from radiation-induced changes in Ag species, $\Delta C(D)$ exhibits a much simpler and more monotonic dose dependence than the PL response.

4. Conclusions

Ag-doped $NaCaPO_4$ ceramics were synthesized and investigated for their X-ray response. Under X-ray irradiation, Ag-doped $NaCaPO_4$ ceramics exhibit signatures consistent with both the RPL and the radiochromic response. In particular, the radiochromic behavior is pronounced: the radiation-induced reflectance change $\Delta C(D)$ over 300–500 nm increases monotonically with irradiation dose. The SPR band at ~400 nm showed the largest change and indicated dose-dependent nanoparticle formation and aggregation. Among the synthesized samples, the 0.3% Ag-doped ceramic exhibited a broad dynamic range from ~1 mGy to 100 Gy, demonstrating excellent performance as a radiochromic material. Whether the predominance of the radiochromic response under X-ray irradiation is an intrinsic property of the material or a secondary effect associated with Ca-site substitution, such as contributions from minor secondary crystalline phases, remains to be clarified and will be investigated further.

Acknowledgments

This work was supported by Grants-in-Aid for Early-Career Scientists (24K17504) and Research Activity Start-up (23K19188) from the Japan Society for the Promotion of Science.

References

1 M. Stabin: Phys. Med. Biol. **51** (2006) R187. https://doi.org/10.1088/0031-9155/51/13/R12
2 M. J. Butson, P. K. N. Yu, T. Cheung, and P. Metcalfe: Mater. Sci. Eng. R Rep. **41** (2003) 61. https://doi.org/10.1016/S0927-796X(03)00034-2
3 W. L. McLaughlin: Radiat. Phys. Chem. (1977) **21** (1983) 359. https://doi.org/10.1016/0146-5724(83)90012-2
4 A. Miller: Radiat. Phys. Chem. **28** (1986) 521. https://doi.org/10.1016/1359-0197(86)90182-7
5 A. Nishikawa, D. Shiratori, T. Kato, D. Nakauchi, N. Kawaguchi, and T. Yanagida: Ceram. Int. **51** (2025) 29409. https://doi.org/10.1016/j.ceramint.2025.04.145
6 D. Shiratori, Y. Isokawa, H. Samizo, G. Okada, N. Kawaguchi, and T. Yanagida: J. Mater. Sci.: Mater. Electron. **30** (2019) 2464. https://doi.org/10.1007/s10854-018-0520-0
7 T. Kato, D. Shiratori, D. Nakauchi, N. Kawaguchi, and T. Yanagida: Jpn. J. Appl. Phys. **59** (2020) 112001. https://doi.org/10.35848/1347-4065/abbc7a
8 M. Iwao, H. Takase, D. Shiratori, D. Nakauchi, T. Kato, N. Kawaguchi, and T. Yanagida: Radiat. Meas. **140** (2021) 106492. https://doi.org/10.1016/j.radmeas.2020.106492
9 D. Shiratori, T. Kato, D. Nakauchi, N. Kawaguchi, and T. Yanagida: Sens. Mater. **33** (2021) 2171. https://doi.org/10.18494/SAM.2021.3317
10 Y. S. Horowitz: Radiat. Prot. Dosim. **47** (1993) 135. https://doi.org/10.1093/oxfordjournals.rpd.a081718
11 N. Salah, P. D. Sahare, S. P. Lochab, and P. Kumar: Radiat. Meas. **41** (2006) 40. https://doi.org/10.1016/j.radmeas.2005.07.026
12 B. Obryk, H. J. Khoury, V. S. de Barros, P. L. Guzzo, and P. Bilski: Radiat. Meas. **71** (2014) 25. https://doi.org/10.1016/j.radmeas.2014.02.002
13 S. W. S. McKeever: Radiat. Prot. Dosim. **109** (2004) 269. https://doi.org/10.1093/rpd/nch302
14 A. Jahn, M. Sommer, W. Ullrich, M. Wickert, and J. Henniger: Radiat. Meas. **56** (2013) 324. https://doi.org/10.1016/j.radmeas.2013.01.069
15 M. Caprioli, L. Delombaerde, M. De Saint-Hubert, L. de Freitas Nascimento, R. De Roover, K. Himschoot, B. van der Heyden, D. Vandenbroucke, P. Leblans, and W. Crijns: Med. Phys. **50** (2023) 1185. https://doi.org/10.1002/mp.16076
16 H. Kimura, F. Nakamura, T. Kato, D. Nakauchi, N. Kawano, G. Okada, N. Kawaguchi, and T. Yanagida: J. Ceram. Soc. Jpn. **126** (2018) 184. https://doi.org/10.2109/jcersj2.17212
17 H. Kawamoto, M. Koshimizu, Y. Fujimoto, and K. Asai: Jpn. J. Appl. Phys. **62** (2023) 010501. https://doi.org/10.35848/1347-4065/ac9cb0
18 H. Tanaka, Y. Fujimoto, M. Koshimizu, T. Yanagida, T. Yahaba, K. Saeki, and K. Asai: Radiat. Meas. **94** (2016) 73. https://doi.org/10.1016/j.radmeas.2016.09.002
19 M. Fuss, E. Sturtewagen, C. De Wagter, and D. Georg: Phys. Med. Biol. **52** (2007) 4211. https://doi.org/10.1088/0031-9155/52/14/013
20 H. Kimura, T. Fujiwara, H. Kato, M. Koshimizu, G. Wakabayashi, Y. Takebuchi, T. Kato, D. Nakauchi, N. Kawaguchi, and T. Yanagida: Sens. Mater. **37** (2025) 599. https://doi.org/10.18494/SAM5442
21 H. Ezawa, T. Kato, Y. Takebuchi, K. Okazaki, K. Ichiba, D. Nakauchi, N. Kawaguchi, and T. Yanagida: Sens. Mater. **37** (2025) 581. https://doi.org/10.18494/SAM5431
22 A. Nishikawa, K. Ichiba, T. Kato, D. Nakauchi, N. Kawaguchi, and T. Yanagida: Sens. Mater. **37** (2025) 569. https://doi.org/10.18494/SAM5429
23 H. Fukushima, D. Shiratori, D. Nakauchi, T. Kato, N. Kawaguchi, and T. Yanagida: Sens. Mater. **34** (2022) 717. https://doi.org/10.18494/SAM3691
24 D. Shiratori, Y. Isokawa, H. Samizo, G. Okada, N. Kawaguchi, and T. Yanagida: J. Mater. Sci.: Mater. Electron. **30** (2019) 2464. https://doi.org/10.1007/s10854-018-0520-0
25 Y. Takebuchi, M. Morioka, Y. Nakashima, K. Tezuka, H. Kimura, S. Otake, and T. Yanagida: Sens. Mater. **37** (2025) 525. https://doi.org/10.18494/SAM5437
26 S. Otake, H. Sakaguchi, Y. Yoshikawa, T. Kato, D. Nakauchi, N. Kawaguchi, and T. Yanagida: Sens. Mater. **36** (2024) 539. https://doi.org/10.18494/SAM4759
27 T. Kato, H. Kimura, K. Okazaki, D. Nakauchi, N. Kawaguchi, and T. Yanagida: Sens. Mater. **35** (2023) 483. https://doi.org/10.18494/SAM4137
28 R. Takahashi, K. Okazaki, D. Nakauchi, T. Kato, N. Kawaguchi, and T. Yanagida: Sens. Mater. **37** (2025) 593. https://doi.org/10.18494/SAM5435
29 G. Okada, C. P. Fernandes, H. Ito, Y. Koguchi, S. Ueno, C. Sawai, W. Kada, K. Watanabe, K. Shinsho, and H. Nanto: Sens. Mater. **37** (2025) 533. https://doi.org/10.18494/SAM5440
30 H. Kawamoto, Y. Fujimoto, and K. Asai: Sens. Mater. **36** (2024) 607. https://doi.org/10.18494/SAM4766

31 A. Nishikawa, D. Shiratori, T. Kato, D. Nakauchi, N. Kawaguchi, and T. Yanagida: Sens. Mater. **36** (2024) 597. https://doi.org/10.18494/SAM4755
32 H. Ito, G. Okada, Y. Koguchi, W. Kada, K. Watanabe, and H. Nanto: Sens. Mater. **36** (2024) 559. https://doi.org/10.18494/SAM4765.
33 D. Shiratori, Y. Isokawa, H. Samizo, N. Kawaguchi, and T. Yanagida: J. Ceram. Soc. Jpn. **127** (2019) 455. https://doi.org/10.2109/jcersj2.19058
34 K. Yamabayashi, K. Okazaki, D. Nakauchi, T. Kato, N. Kawaguchi, and T. Yanagida: Sens. Mater. **37** (2025) 627. https://doi.org/10.18494/SAM5434
35 C. G. Soares: Radiat. Meas. **41** (2006) S100. https://doi.org/10.1016/j.radmeas.2007.01.007
36 B. V. Ratnam, M. Jayasimhadri, G. Bhaskar Kumar, K. Jang, S. S. Kim, Y. I. Lee, J. M. Lim, D. S. Shin, and T. K. Song: J. Alloys Compd. **564** (2013) 100. https://doi.org/10.1016/j.jallcom.2013.01.203
37 A. D. Vartha, P. R. Patankar, P. D. Sahare, M. K. Jite, S. D. Dhole, and N. T. Mandlik: Appl. Radiat. Isot. **227** (2025) 112261. https://doi.org/10.1016/j.apradiso.2025.112261
38 C. Qin, Y. Huang, L. Shi, G. Chen, X. Qiao, and H. J. Seo: J. Phys. D: Appl. Phys. **42** (2009) 185105. https://doi.org/10.1088/0022-3727/42/18/185105
39 Z. Yang, G. Yang, S. Wang, J. Tian, X. Li, Q. Guo, and G. Fu: Mater. Lett. **62** (2008) 1884. https://doi.org/10.1016/j.matlet.2007.10.030
40 D. Shiratori, T. Kato, D. Nakauchi, N. Kawaguchi, and T. Yanagida: Sens. Mater. **33** (2021) 2171. https://doi.org/10.18494/SAM.2021.3317
41 R. Achagar, A. Elmakssoudi, A. Thoume, M. Dakir, A. Elamrani, Y. Zouheir, M. Zahouily, Z. Ait-Touchente, J. Jamaleddine, and M. M. Chehimi: Appl. Sci. **12** (2022) 5487. https://doi.org/10.3390/app12115487
42 L. Xu, N.-P. Liu, H.-L. An, W.-T. Ju, B. Liu, X.-F. Wang, and X. Wang: Ultrason. Sonochem. **89** (2022) 106147. https://doi.org/10.1016/j.ultsonch.2022.106147
43 H. Aouad, M. Maazaz, and I. Belharouak: Mater. Res. Bull. **35** (2000) 2457. https://doi.org/10.1016/S0025-5408(00)00452-9
44 M. El Masloumi, V. Jubera, S. Pechev, J. P. Chaminade, J. J. Videau, M. Mesnaoui, M. Maazaz, and B. Moine: J. Solid State Chem. **181** (2008) 3078. https://doi.org/10.1016/j.jssc.2008.07.040
45 S. W. S. McKeever, S. Sholom, and N. Shrestha: Radiat. Meas. **123** (2019) 13. https://doi.org/10.1016/j.radmeas.2019.02.009
46 Y. Miyamoto, T. Yamamoto, K. Kinoshita, S. Koyama, Y. Takei, H. Nanto, Y. Shimotsuma, M. Sakakura, K. Miura, and K. Hirao: Radiat. Meas. **45** (2010) 546. https://doi.org/10.1016/j.radmeas.2010.01.012
47 W. Zheng and T. Kurobori: J. Lumin. **131** (2011) 36. https://doi.org/10.1016/j.jlumin.2010.08.024
48 I. Belharouak, F. Weill, C. Parent, G. Le Flem, and B. Moine: J. Non-Cryst. Solids **293–295** (2001) 649. https://doi.org/10.1016/S0022-3093(01)00843-2
49 D. Manikandan, S. Mohan, and K. G. M. Nair: Mater. Res. Bull. **38** (2003) 1545. https://doi.org/10.1016/S0025-5408(03)00165-X
50 K. Ren, X. Xu, Z. Yao, X. Chen, T. Hu, P. Li, X. Fan, J. Du, X. Qiao, and G. Qian: Phys. Chem. Chem. Phys. **22** (2020) 21307. https://doi.org/10.1039/D0CP03828H
51 H. Kawamoto, Y. Fujimoto, and K. Asai: J. Lumin. **288** (2025) 121562. https://doi.org/10.1016/j.jlumin.2025.121562
52 S. Sholom and S. W. S. McKeever: Radiat. Meas. **163** (2023) 106924. https://doi.org/10.1016/j.radmeas.2023.106924
53 P. Sharma, R. Singhal, R. Vishnoi, D. C. Agarwal, M. K. Banerjee, S. Chand, D. Kanjilal, and D. K. Avasthi: Plasmonics **13** (2018) 669. https://doi.org/10.1007/s11468-017-0559-4
54 J. A. Jiménez, S. Lysenko, G. Zhang, and H. Liu: J. Electron. Mater. **36** (2007) 812. https://doi.org/10.1007/s11664-007-0142-4
55 P. Casolaro: Appl. Sci. **11** (2021) 2132. https://doi.org/10.3390/app11052132
56 S. Aldelaijan, N. Tomic, P. Papaconstadopoulos, J. Schneider, J. Seuntjens, S. Shih, D. Lewis, and S. Devic: Med. Phys. **45** (2018) 488. https://doi.org/10.1002/mp.12689
57 M. Z. Mohyedin, H. M. Zin, S. Hashim, D. A. Bradley, S. Aldawood, M. Alkhorayef, A. Sulieman, and A. T. Abdul Rahman: Radiat. Phys. Chem. **200** (2022) 110312. https://doi.org/10.1016/j.radphyschem.2022.110312